Enhancing humoral immunity via sustained-release implantable microneedle patch vaccination

Archana V. Boopathy[a], Anasuya Mandal[a,b], Daniel W. Kulp[c,d,e], Sergey Menis[c,e,f], Nitasha R. Bennett[a], Hannah C. Watkins[a], Wade Wang[a,b,g], Jacob T. Martin[a], Nikki T. Thai[a], Yanpu He[a,b], William R. Schief[c,e,f,h], Paula T. Hammond[a,b,1], and Darrell J. Irvine[a,c,g,h,i,j,k,1]

[a]Koch Institute for Integrative Cancer Research, Massachusetts Institute of Technology, Cambridge, MA 02139; [b]Department of Chemical Engineering, Massachusetts Institute of Technology, Cambridge, MA 02139; [c]Center for HIV/AIDS Vaccine Immunology and Immunogen Discovery, The Scripps Research Institute, La Jolla, CA 92037; [d]Vaccine and Immunotherapy Center, The Wistar Institute, Philadelphia, PA 19104; [e]International AIDS Vaccine Initiative Neutralizing Antibody Center, The Scripps Research Institute, La Jolla, CA 92037; [f]Department of Immunology and Microbial Science, The Scripps Research Institute, La Jolla, CA 92037; [g]Institute for Soldier Nanotechnologies, Massachusetts Institute of Technology, Cambridge, MA 02139; [h]Ragon Institute of Massachusetts General Hospital, Massachusetts Institute of Technology and Harvard, Cambridge, MA 02139; [i]Department of Biological Engineering, Massachusetts Institute of Technology, Cambridge, MA 02139; [j]Department of Material Science and Engineering, Massachusetts Institute of Technology, Cambridge, MA 02139; and [k]Howard Hughes Medical Institute, Massachusetts Institute of Technology, Cambridge, MA 02139

Edited by Rino Rappuoli, GlaxoSmithKline, Siena, Italy, and approved June 27, 2019 (received for review February 7, 2019)

Sustained exposure of lymphoid tissues to vaccine antigens promotes humoral immunity, but traditional bolus immunizations lead to rapid antigen clearance. We describe a technology to tailor vaccine kinetics in a needle-free platform translatable to human immunization. Solid pyramidal microneedle (MN) arrays were fabricated with silk fibroin protein tips encapsulating a stabilized HIV envelope trimer immunogen and adjuvant, supported on a dissolving polymer base. Upon brief skin application, vaccine-loaded silk tips are implanted in the epidermis/upper dermis where they release vaccine over a time period determined by the crystallinity of the silk matrix. Following MN immunization in mice, Env trimer was released over 2 wk in the skin, correlating with increased germinal center (GC) B cell responses, a ∼1,300-fold increase in serum IgG titers and a 16-fold increase in bone marrow (BM) plasma cells compared with bolus immunization. Thus, implantable MNs provide a practical means to substantially enhance humoral immunity to subunit vaccines.

microneedles | antibody response | vaccine delivery

The majority of licensed vaccines are thought to protect through the induction of protective antibodies, and antibody responses are considered crucial for many outstanding vaccine challenges. For example, preclinical animal studies predict that an HIV vaccine capable of eliciting broadly neutralizing antibodies (bnAbs), defined as antibodies that neutralize diverse isolates of the circulating virus, would provide sterilizing immunity to infection (1). However, bnAbs often have levels of somatic hypermutation substantially greater than that elicited by typical vaccines and unusual structural features (2–4), which may require highly active germinal center (GC) responses. Such a vaccine will thus likely need both appropriate immunogen design and optimization of multiple steps of the humoral response to produce durable levels of bnAbs.

Recently, vaccine kinetics—the temporal profile of antigen and inflammatory cues during immunization—have been shown to impact the humoral response to subunit vaccines. Delivery of HIV antigens with adjuvants over 2 wk in mice either by repeated injections or via implanted miniosmotic pumps resulted in enhanced humoral responses relative to traditional bolus immunization due to increased antigen availability during GC induction (5, 6). Similarly, intradermal fractional dosing of an inactivated polio vaccine in rats resulted in 10-fold higher serum titers (7). In nonhuman primates, sustained HIV envelope antigen delivery over 2 wk using osmotic pumps induced higher tier 2 autologous NAbs than equivalent bolus injections (8). While these studies provide proof of principle, osmotic pump implantation or immunizations through a half-dozen injections are impractical for prophylactic vaccination.

Microneedle (MN) skin patches are an attractive platform to control vaccine kinetics. MNs are arrays of microscale solid projections that mechanically pierce the stratum corneum to deposit vaccines in the epidermis/dermis and have been demonstrated as a promising modality for needle- and pain-free vaccine administration in early clinical trials (9–11). Motivated by these attributes of MNs, we recently reported a design for MNs with implantable biodegradable polymer tips (12). The model antigen ovalbumin (OVA) was encapsulated in molded MN tips composed of regenerated silk fibroin protein supported on a dissolving poly(acrylic acid) (PAA) polymer backing. Silk proteins form solid matrices on drying with varying degrees of β-sheet crystallinity, which can be used to regulate the release rate of entrapped biologics (13, 14). On application of these composite MNs to the skin for 5–10 min, the PAA backing rapidly swells and dissolves, allowing silk tips to detach and remain implanted in the epidermis/upper dermis following patch removal. Subsequently, swelling and proteolysis of the silk matrix allows the entrapped vaccine to be released over an extended period (12). A significant limitation of this initial patch fabrication strategy was that much of the antigen cargo leached from the silk tip into the PAA backing during processing such that only a very small fraction (∼5%) of the total dose was loaded into the silk tip. In addition, while MN delivery improved immune responses to the highly immunogenic very stable model antigen OVA, a concern remained that silk might

Significance

Vaccine kinetics, the timing of antigen and/or adjuvant delivery to lymphoid organs, have recently been shown to substantially influence immune responses to subunit vaccines, but strategies to control vaccine kinetics in a clinically translatable manner are still lacking. MNs are arrays of solid micron-sized projections that have been utilized in early clinical trials for vaccine delivery. Here, we investigated whether implantable MN skin patches could be used to control vaccine kinetics. We show that sustained intradermal release of an HIV subunit vaccine from MNs enhanced GC responses and significantly improved humoral immunity compared with traditional bolus injections. The findings of this study have strong translational relevance as MNs, such as described here, can provide rapid needle-free vaccine administration.

Author contributions: A.V.B., W.R.S., P.T.H., and D.J.I. designed research; A.V.B., A.M., N.R.B., H.C.W., W.W., J.T.M., and N.T.T. performed research; A.V.B., A.M., H.C.W., W.W., J.T.M., and D.J.I. analyzed data; D.W.K., S.M., and Y.H. contributed new reagents/analytic tools; and A.V.B., W.R.S., P.T.H., and D.J.I. wrote the paper.

The authors declare no conflict of interest.

This article is a PNAS Direct Submission.

[1]To whom correspondence may be addressed. Email: hammond@mit.edu or djirvine@mit.edu.

This article contains supporting information online at www.pnas.org/lookup/suppl/doi:10.1073/pnas.1902179116/-/DCSupplemental.

denature bona fide vaccine antigens, such as the HIV trimer, which have complex and often fragile quaternary structures. Here, we addressed these challenges by combining an improved silk MN fabrication approach with the use of an HIV trimer immunogen engineered for high stability. Together, these advances allowed MNs to be fabricated that released a structurally intact envelope trimer over ~2 wk in mice and greatly enhanced humoral immunity.

Results

Implantable Silk MN Skin Patch Fabrication for Sustained Release of Intact Antigen. For the antigen, we focused on gp140 trimers based on BG505 SOSIP, a stabilized native-like trimer with an antigenicity profile mirroring the native viral envelope (15, 16). Motivated by the expression patterns of Toll-like receptors (TLRs) in keratinocytes, Langerhans cells, and dermal dendritic cells (17, 18), we evaluated the TLR2 agonist pam$_3$CSK$_4$ and the TLR3 agonist polyI:C as candidate adjuvants for this skin-targeting vaccine and found that the combination of these 2 adjuvants both strongly recruited immune cells to the skin and elicited pronounced lymphadenopathy in draining lymph nodes (LNs) (*SI Appendix*, Fig. S1). To fabricate MNs containing these vaccine components, silk fibroin with M_W ~ 22 kDa (*SI Appendix*, Fig. S2*A*) was isolated from *bombyx mori* cocoons following established procedures. As shown in Fig. 1*A*, MNs were fabricated by depositing an aqueous solution of vaccine and regenerated silk into poly(dimethyl siloxane) molds and drying, followed by methanol vapor annealing to promote silk crystallization in situ, and application of aqueous PAA, which, upon drying, formed a mechanically robust polymer backing that would quickly dissolve on application to the skin. As reported by prior studies of silk processing (19–21), annealing of silk matrices with methanol vapor promoted β-sheet crystallinity as evidenced by fluorescence and FTIR analysis (*SI Appendix*, Fig. S2 *B–D*). Methanol vapor annealing and optimization of silk:trimer mass ratio to a value of 10:1 led to the formation of MNs with the trimer, pam$_3$CSK$_4$, and polyI:C distributed in the silk tips with no vaccine in the PAA backing (Fig. 1*B*).

A key issue for developing a sustained release formulation for vaccines is preservation of structural integrity of the immunogen. We selected silk as the carrier biomaterial as fibroin matrices have been reported to maintain biologics in a bioactive state even following drying, acting as a lyoprotectant (22, 23). To assess the suitability of silk to encapsulate and release intact trimers, we first encapsulated a BG505 SOSIP trimer in silk MNs, dissolved in PBS/Tween 20 solution, and probed the recovered protein using structure-specific monoclonal antibodies (mAbs) by ELISA. As a control, the unmanipulated trimer was incubated in the same tween solution before ELISA. As shown in Fig. 1*C*, the BG505 SOSIP trimer recovered from MNs showed significantly lower binding compared with the starting trimer S for all of the mAbs tested, suggesting substantial loss of trimer structural integrity. We carried out preliminary tests of attempting to solve this immunogen instability issue via the incorporation of stabilizing excipients, such as trehalose and sucrose in the MN preparation, but this approach was problematic as the excipients tended to accelerate antigen release kinetics from silk. To overcome this challenge, we employed a recently described hyperstabilized BG505 SOSIP trimer, termed MD39, which incorporates multiple mutations promoting optimal protomer packing and exhibits considerably higher thermal stability than BG505 SOSIP (24). In contrast to findings with SOSIP, MD39 trimers recovered from MNs showed high levels of binding to the bnAbs PGT121, PGT151, VRCO1, and 35022 with only minor losses in binding to PGT145 (Fig. 1*C*). In addition, nonbnAbs 14e, B6, 39F, and 4025 that recognize epitopes exposed only in unfolded/nonnative trimers, such as the V3 loop showed low binding to both the starting MD39 trimer and the MN-recovered antigen (Fig. 1*D* and *SI Appendix*, Fig. S3). MN patches containing BG505 SOSIP or MD39 trimer were prepared and dissolved to recover the encapsulated trimer as in Fig. 1*C*, and the released trimer was analyzed by FPLC. As shown in *SI Appendix*, Fig. S4, while untreated SOSIP eluted at ~8.75 mL, SOSIP recovered from MNs had a major peak eluting at the column void volume (~7.5 mL, *SI Appendix*, Fig. S4*A*). By contrast, untreated MD39 or the trimer recovered from silk MNs exhibited similar profiles with a major peak indicative of an intact trimer at ~8.75 mL (*SI Appendix*, Fig. S4*B*). These data suggest BG505 SOSIP undergoes aggregation when encapsulated in silk, in contrast to

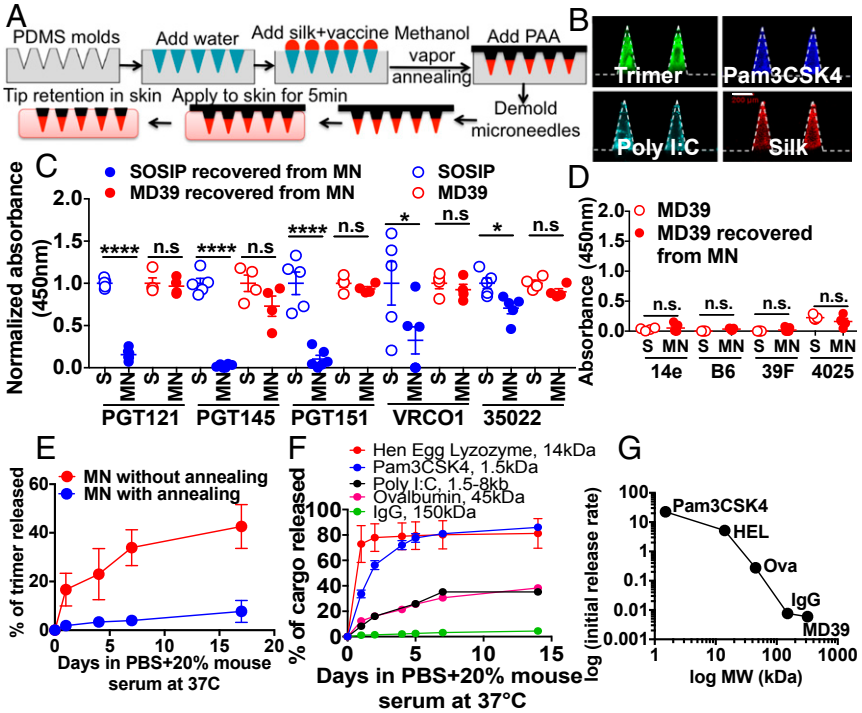

Fig. 1. Formulation of implantable silk MNs for the slow release of HIV envelope trimers with intact structural integrity. (*A*) Schematic of MN preparation and application to skin. (*B*) Representative confocal microscopy images of MN containing fluorescently labeled MD39 trimer, pam$_3$CSK$_4$, polyI:C, and silk (Scale bar, 200 μm). (*C*) Antigenicity profiles of SOSIP or MD39 trimers extracted from as-prepared silk MNs were evaluated by capture of recovered trimer on plates followed by ELISA analysis with a panel of bnAbs, normalizing binding to that observed with equivalent amounts of unmanipulated soluble trimer protein (S). (*D*) Antigenicity profile of MD39 trimer evaluated by ELISA with a panel of nonbnAbs. (*E*) In vitro release of a MD39 trimer at 37 °C in PBS with 20% mouse serum quantified by ELISA. (*F*) In vitro release of fluorescent cargos of different MWs at 37 °C in PBS with 20% mouse serum from methanol-annealed silk MNs. (*G*) Plot of early release rate of cargo vs. MWW based on data in *E* and *F*. n = 5/group in *C–F*; $^*P < 0.05$, $^{****}P < 0.0001$, n.s. stands for not significant, and Student's t test in *C* and *D*.

the stabilized MD39 trimer. We thus focused on MD39 as the immunogen for further studies. In vitro rates of the trimer release from silk MNs exposed to serum were significantly decreased by silk annealing (Fig. 1*E*). Measurement of the amount of MD39 trimer released from annealed MN patches over time using the quaternary structure-sensitive monoclonal antibodies PGT145, PGT151, and PGT121 revealed similar release kinetics, suggesting the released trimer was largely intact (*SI Appendix*, Fig. S5). Examining release rates of adjuvants and other model globular proteins showed a clear trend of decreasing release rates from annealed MNs with increasing cargo molecular weight (MW) (Fig. 1 *F* and *G*).

MN Delivery Results in Sustained Trimer Retention in Vaccine Draining LNs and Promotes GC Formation. We previously showed that a 5–10-min application of PAA-supported MNs to the skin leads to swelling and dissolution of the PAA with tip implantation in the epidermis/upper dermis (12). Preliminary experiments using this procedure showed that the majority of patches delivered 100% of the loaded vaccine dose with this application regimen (*SI Appendix*, Fig. S6). To determine the in vivo kinetics of trimer release, MNs coencapsulating adjuvants and AlexaFluor-labeled MD39 in silk tips were applied to the ear skin of mice. Antigen retention in the skin was tracked longitudinally by confocal imaging and whole-animal fluorescence. Immediately following patch application, regular arrays of tips containing labeled MD39 could be observed in the epidermis/dermis of treated mice (Fig. 2*A*), and the total antigen signal at the application site decayed steadily over 14 d (Fig. 2*B*). By contrast, the trimer administered together with the adjuvant as a traditional bolus intradermal (i.d.) injection exhibited rapid clearance over a few days in vivo (Fig. 2*B*).

To assess the impact of sustained vaccine release on trafficking of the antigen to the draining LNs (dLNs), mice were immunized via patches or bolus i.d. injection, and dLNs were harvested 7- or 14-d postimmunization. Swelling of dLNs followed distinct kinetics with lymphadenopathy increasing through day 14 for animals receiving the slow-release MN, while bolus immunization led to a peak in dLN mass at day 7 followed by steady contraction (Fig. 2*C*). Trimer fluorescence in dLNs was comparable on day 7 for the MN and bolus immunizations, but, at day 14, the accumulated MD39 present in the nodes continued to increase while levels of the bolus-injected antigen remained relatively constant (Fig. 2*D*). MN delivery also resulted in a substantially greater proportion (21.2 ± 4.65%) of the LN-localized antigen colocalized with the follicular dendritic cell (FDC) network for ready access by responding B cells, compared with 7.8 ± 0.45% following bolus delivery (Fig. 2 *E* and *F*). Trimer accumulation was dependent on inclusion of adjuvants independent of the route of delivery (*SI Appendix*, Fig. S7).

We next characterized the impact of MN immunization on GC responses to the MD39 trimer. We analyzed trimer-specific GC follicular helper T cells (Tfh) by an activation-induced marker assay (25) (Fig. 3 *A* and *B* and *SI Appendix*, Fig. S8). Trimer-specific Tfh cells were higher at day 7 for bolus vaccination, but while the response contracted from day 7 onward in the bolus-immunized animals, it continued to increase to a similar peak of expansion on day 14 in MN-immunized mice. GC B cells showed delayed expansion in MN compared with bolus immunization but peaked at approximately twice the maximal level observed in the bolus-immunized group (Fig. 3 *C* and *D* and *SI Appendix*, Fig. S9). Thus, MN immunization elicited comparable Tfh responses but enhanced GC B cell induction in dLNs.

MN Delivery Promotes Durable Antibody Responses. To determine the effect of sustained antigen release on antibody responses, mice were primed and boosted with MNs or bolus intradermal injections, and humoral responses were evaluated over time. As shown in Fig. 4*A*, sustained vaccine release from MNs resulted in a 1,300-fold higher serum MD39-specific IgG titer than equivalent intradermal injections at week 13 and were sustained for months

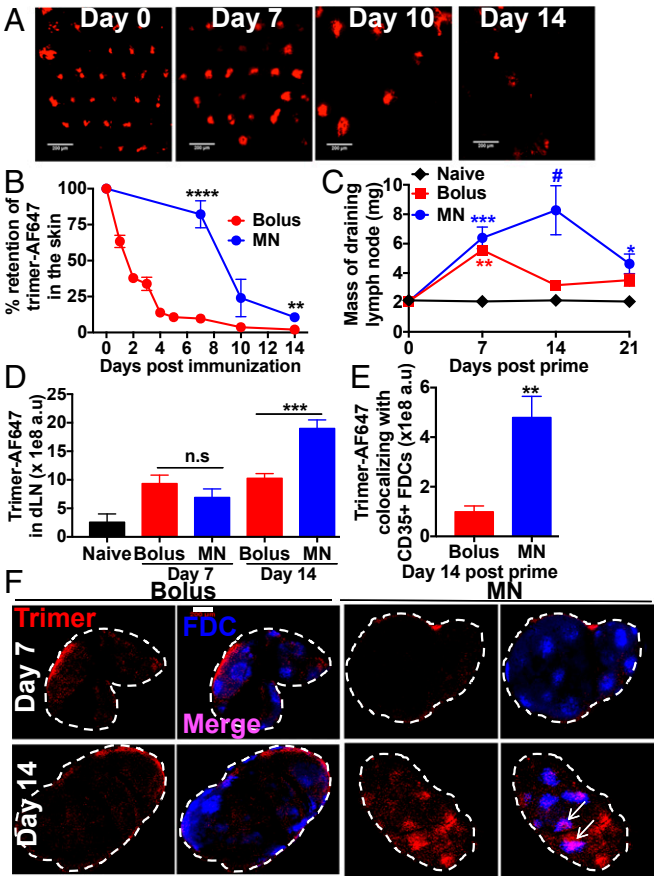

Fig. 2. MNs promote and sustain trimer delivery to LNs. Groups of balb/c mice (n = 4/group) were treated on the ear skin with MN patches delivering Alexafluor-labeled MD39 trimer together with an adjuvant or received intradermal bolus injections of the same antigen/adjuvant doses. (*A*) Representative confocal images of the MN patch application site visualizing trimer in the skin over time. (*B*) Decay kinetics of a fluorophore-antigen signal in skin following MN or i.d. bolus immunization. (*C*) Mass of dLNs following immunization. (*D*) Quantification of labeled trimer accumulation in dLNs determined by confocal imaging of serial LN sections (n = 4 LNs for naive and MN groups and n = 6 LNs for the bolus group). (*E*) Quantification of trimer fluorescence colocalizing with FDCs (n = 4 LNs/group). (*F*) Representative confocal images of LN sections showing trimer (in red) accumulation relative to FDC networks (in blue) at days 7 and 14. $^{*}P < 0.05$, $^{**}P < 0.01$, $^{***}P < 0.001$, $^{****}P < 0.0001$, $^{\#}P < 0.0001$ vs. naive and bolus, n.s. not significant, unpaired Student's t test in *B*, *D*, and *E*, and 2-way ANOVA with Sidak's posttest in *C* (Scale bars, 200 μm in *A* and *F*).

later, but no response to silk itself was detectable (*SI Appendix*, Fig. S10). As skin immunization can promote distal mucosal immunity (26, 27), we assessed mucosal IgG and IgA. MN immunization showed a trend toward elevated vaginal IgG and IgA but did not reach statistical significance (*SI Appendix*, Fig. S11). By contrast, quantification of trimer-specific IgG ASCs at 8-wk post-boost revealed enhanced frequencies of antigen-specific plasma cells (Fig. 4 *B* and *C*) and memory B cells (Fig. 4 *D* and *E*) in the BM in MN-immunized animals. We finally evaluated the relative importance of sustained release of antigen vs. adjuvant in enhancing antibody responses. Mice were immunized with MD39 trimer and the adjuvant with the adjuvant either encapsulated in MN or injected as a bolus at the same site immediately following MN application, and slow release of antigen, adjuvant, or both, were compared. We also tested the antibody response to MN-released trimer in the absence of adjuvants. Slow release of the antigen and adjuvant together gave the highest IgG titers but no higher than a slow release antigen in the presence of a bolus-administered

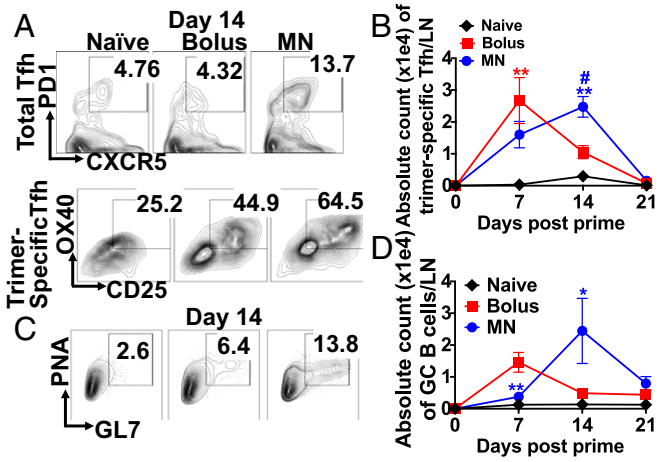

Fig. 3. Trimer delivery via MNs promotes GC responses. BALB/c mice (n = 6/group) were immunized with 5-μg MD39 trimer and adjuvants by MN patches or equivalent i.d. injections (bolus) and killed at 7, 14, or 21 d later for flow cytometry analysis of dLNs. (*A*) Representative flow cytometry plots of trimer-specific Tfh (gated as $OX40^+CD25^+PDL1^+$ of $B220^-CD4^+CD44^+CXCR5^+PD1^+$ Tfh) on day 14 post prime and (*B*) quantification over time. (*C*) Representative flow cytometry plots of GC B cells ($B220^+$ IgD^{low} PNA^+GL7^+) on day 14 and (*D*) quantification over time. *$P < 0.05$, **$P < 0.01$, # $P < 0.0001$, and 1-way ANOVA at each time point with Tukey's posttest. In *D*, * and ** are bolus vs. MN, in *B*, ** vs. naive at day 7, ** vs. bolus and # vs. naive at day 14. Shown is 1 representative of 2 separate experiments.

adjuvant, suggesting that sustained antigen release has the greatest impact on vaccine response (Fig. 4 *F* and *G*).

Discussion

Generation of neutralizing antibodies is the protective mechanism of action for many licensed vaccines. Development of bnAbs is also thought to be a critical determinant of success for a prophylactic HIV vaccine (1, 28, 29). Progress in HIV vaccine development has focused on appropriate immunogen design, choice of adjuvant, dosage, and route of vaccine administration to achieve bnAb generation. In addition to these much studied factors, the role of vaccine kinetics in modulating humoral immune response has recently been revealed by studies employing repeated injections (6, 7) or through continuous-delivery osmotic pumps (5, 8) in mice, rats, and nonhuman primates. However, implementation of such a repeated injection schedule or surgical implantation of vaccine delivery pumps is not feasible for global distribution of prophylactic vaccines. Therefore, we were motivated to develop a noninvasive MN device as a scalable platform for prophylactic HIV vaccine delivery.

Here, we engineered implantable MNs designed to sustain release the HIV envelope trimer immunogens over 2 wk by utilizing silk fibroin protein to encapsulate the vaccine. Upon brief 5-min application to the skin, silk tips containing the vaccine are embedded in the skin and release the vaccine over time. In vitro release studies demonstrated maintenance of the structural integrity of the antigen and a MW-dependent release over time from annealed silk MNs. Sustained release of the vaccine from MNs during the prime resulted in increased local retention in the skin and a 3-fold increase in colocalization with FDCs in dLNs, correlating with an increased priming of GC B cells compared with bolus injection. As GCs can be active for several weeks postimmunization, facilitating antigen availability on a timescale that syncs with the GC time course could result in enhanced immune responses. MN immunization led to 1,300-fold higher antibody titers compared with equivalent bolus injections at 1-mo postboost.

HIV trimer immunogens were released from an annealed silk MN at a steady slow rate in the presence of serum in vitro. Interestingly, antigen release kinetics from implanted MN tips in vivo were distinct with a slow release of ~20% of the delivered antigen over the first ~8 d, followed by an apparent acceleration in antigen release over the subsequent week. The mechanisms underlying this nonmonotonic release behavior are still under investigation, but we suspect the silk may reach a critical swelling/degradation threshold in vivo that allows a transition to more rapid diffusion-regulated release at later times. Although the silk MN patches released the incorporated TLR agonist adjuvants faster than the trimer immunogen, humoral responses elicited by a patch-delivered antigen combined with bolus adjuvant injection vs. antigen and adjuvant both released over time from patches were equivalent. By contrast, bolus antigen injection combined with a patch-released adjuvant elicited much lower IgG titers. These results suggest that sustained release of an antigen but not an adjuvant is critical for priming maximal antibody responses.

Silk fibroin is a natural biopolymer with attractive properties for use as a biomaterial and has been explored in diverse applications ranging from tissue engineering to drug delivery (30, 31). The ability of silk to be processed using aqueous solutions at low temperatures and for its crystallinity to be modulated by simple process variables has particularly motivated the application of silk as a drug delivery matrix (14, 32). Prior studies have demonstrated the ability of silk matrices to encapsulate and release intact and bioactive cytokines (33, 34), antibodies (35), and enzymes (36, 37). However, the Env trimer presents a particularly challenging cargo due to its large size, noncovalent assembly, and multimeric nature, coupled with the paramount importance of 3D structural integrity for elicitation of antibody responses that could recognize the native virus. We found that a mildly stabilized BG505 SOSIP trimer was partially denatured following encapsulation and release from silk matrices. However, this problem was overcome by leveraging the fact that the HIV immunogen design field has invested enormous effort in designing more stable and robust engineered trimers. The hyperstabilized MD39 trimer (24) showed nearly perfect retention of its folded structure following silk entrapment, indicating the value of engineering both the encapsulating matrix and the cargo to be encapsulated.

We were motivated to explore strategies for sustained vaccine release using MNs based on the promise of MN technologies for drug and vaccine delivery. MN patches of diverse design have been intensively studied in preclinical studies over the past 10 y (38). Recently, Phase I clinical trials have shown MNs as a promising alternative to traditional injections for the delivery of vaccines (9, 11). These pioneering clinical studies have focused on rapid release of a biologic from MNs upon application to the skin but set the stage for next-generation approaches, such as the sustained-release implantable MNs described here.

In conclusion, we show here that sustained vaccine release achieved through implantable MN skin patches enhances multiple aspects of humoral immunity, including GC B cell differentiation, class-switched antibody titers, and induction of long-lived plasma cells. The ability of silk MN patches to enhance these multiple facets of humoral immunity in a needle-free platform amenable to rapid vaccination should be of interest for diverse infectious disease applications.

Materials and Methods

Materials. Regenerated silk fibroin solution was prepared from *B. mori* silk cocoons (Aurora Silk) (39). PolyI:C high molecular weight (HMW), pam_3CSK_4, polyI:C fluorescein, pam_3CSK_4 rhodamine, AF647-labeled ovalbumin, and rabbit anti-goat IgG (H+L) AF647 were purchased from Life Technologies. Hen egg lysozyme (Sigma-Aldrich) was labeled with NHS-functionalized AlexaFluor 647 (Life Technologies) according to the manufacturer's instructions.

MD39 and BG505 SOSIP Trimers. Engineered BG505 SOSIP and MD39 gp140 trimers containing C-terminal histags were prepared as previously described (24). Briefly, trimer genes were mixed with a plasmid containing furin protease (2 trimer: 1 furin ratio) and 293fectin, then transfected into FreeStyle 293F cells. After 7 d, trimers secreted from 293F cells were purified by affinity chromatography using HisTrap columns (GE Healthcare) followed by size-exclusion chromatography (SEC) on a S200 Increase column (GE Healthcare) in PBS. MW of the trimer was confirmed by SEC multiangle light scattering using DAWN HELEOS II and Optilab T-rEX instruments (Wyatt Technology) and concentrated to 1 mg/mL.

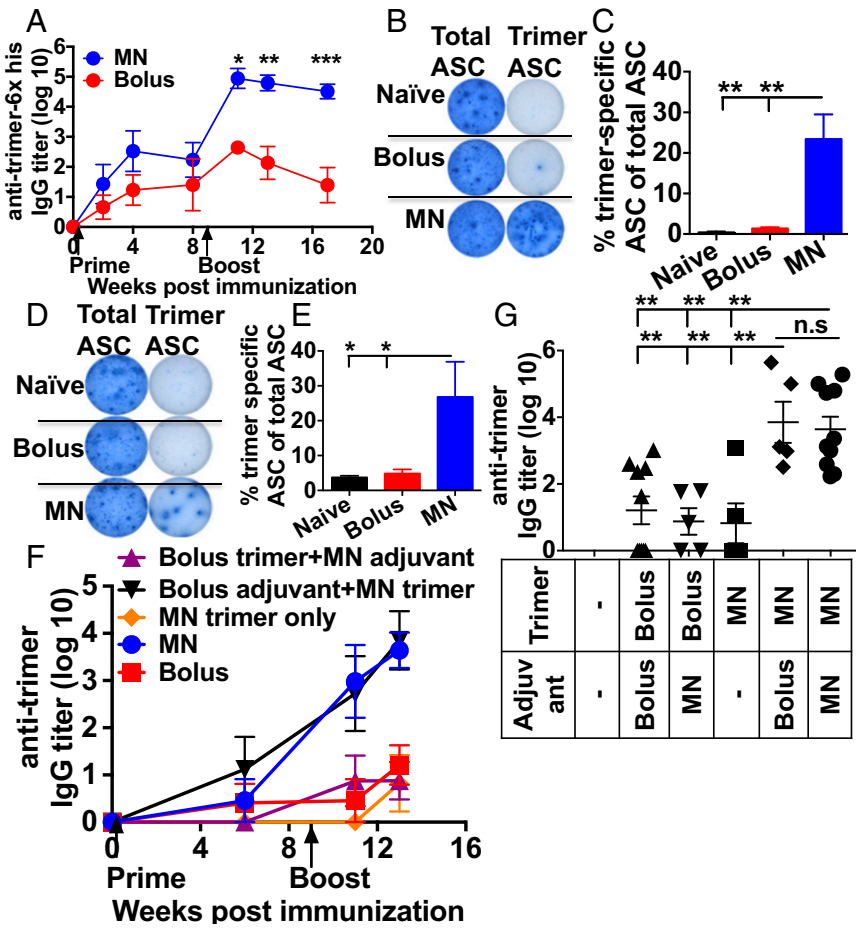

Fig. 4. MNs sustain strong trimer-specific humoral responses. (*A–F*) BALB/c mice (n = 5/group) were immunized on days 0 and 60 with a 5-μg MD39 trimer and adjuvants by bolus i.d. immunization or MN patches. Shown are ELISA analyses of anti-trimer-His serum IgG responses over time (*A*), representative ELISPOT plate images measuring total IgG (*Left* column) or trimer-specific IgG (*Right* column) for long-lived plasma cells (*B*) and memory B cells (*D*). Mean percentages of trimer-specific antibody-secreting cells (ASCs) relative to the total number of ASCs in the BM in *B* and *D* is quantified in *C* and *E*, respectively. (*F* and *G*) BALB/c mice were immunized with bolus or MN immunizations on days 0 and 60; shown are ELISA analyses of antitrimer serum IgG responses over time in *F* and data from individual animals at 1-mo post boost in *G*. $*P < 0.05$, $**P < 0.01$, $***P < 0.001$, n.s. not significant, 2-way ANOVA with Sidak's posttest in *A*, and 1-way ANOVA with Tukey's posttest in *C*, *E*, and *G*. Data shown are from 1 representative of 2 independent experiments.

Preparation of MN Patches. MNs were fabricated from polydimethylsiloxane (PDMS) molds (Sylgard 184, Dow Corning) machined by laser ablation to create pyramidal shaped micron-sized arrays (250 μm at the base, 650 μm in height with a pitch of 250 μm as a 9 × 9 array) as previously described (12). Silk solution (6 wt%) containing vaccine (5-μg MD39 antigen and 2.5-μg each of adjuvants polyI:C HMW and pam_3CSK_4) in PBS (total volume 2.6 μL) for the whole array was drop cast into cavities using a syringe pump (NE1000, New Era Pump Systems, Inc., single channel, flow rate 0.8 μL/min). Molds containing vaccine were air dried for 8 h at 25 °C. Methanol vapor annealing was performed by placing molds inside a dessicator containing 100-mL methanol (Sigma-Aldrich) in a beaker and set under vacuum for 24 h at 25 °C. Molds were then backfilled with 35 wt% PAA (MW 250 kDa, Sigma-Aldrich) by centrifugation (10 min,1,600 rpm) followed by drying in a dehumidifier at 25 °C for 3 d. Dried MNs were demolded and stored at 25 °C until use.

Trimer Antigenicity Analysis. Antigenic profiles of the trimer were quantified by ELISA. PDMS molds were prepared with trimers and adjuvants as above and subject to methanol vapor annealing. After 24 h, molds were incubated in release media (0.1% Tween 20 in PBS, pH 7.4) for 1 h at 37 °C, 150 rpm. Soluble trimer was also subject to the same treatment. Briefly, Maxisorp 96-well plates (Nunc) were coated with rabbit anti-6xHis antibody (Genscript, A00174). Serial dilutions of the trimer released from molds or soluble trimer were added. Detection antibodies (bnAbs: PGT121, PGT151, VRCO1, 35022, and nonbnAbs:14e, B6, 39F, and 4025) were added at 0.1 μg/mL followed by secondary detection with goat anti-human IgG HRP (1:5,000, BioRad, 5172–2504). Trimer denatured by water-bath sonication for 30 min served as a positive control for binding to nonbnabs.

Quantification of In Vitro Release from Silk MNs. Silk MNs were prepared with different antigens mixed with a constant dose of polyI:C and pam_3CSK_4 and subjected to methanol annealing. The MN tips were incubated in 100-μL PBS pH 7.4 with 20% mouse serum at 37 °C for 15 d with media replaced every day. Release of fluorescent pam_3CSK_4, HEL, IgG, OVA, and polyI:C were tracked by fluorescence spectroscopy on aliquots of the MN supernatants over time using a Tecan M1000 plate reader, calibrated by reference standard solutions of each molecule. Unlabeled MD39-6x His tag was quantified by passing through a Ni-NTA column (Qiagen, 30210), followed by Amicon 10K MW cutoff concentration and sandwich ELISA capturing the trimer with rabbit anti-6xHis antibody and using gp160-specific monoclonal antibodies PGT121, PGT145, or PGT151 as detection agents followed by secondary detection with goat anti-human IgG HRP (1:5,000, BioRad, 5172–2504).

Immunizations. All animal studies were conducted in accordance with an Institutional Animal Care and Use Committee-approved protocol following federal, state, and local guidelines at the Massachusetts Institute of Technology (MIT). Female balb/c mice (6–8 wk old, Jackson Laboratories) were immunized with 5-μg MD39 trimer, 2.5-μg polyI:C, and 2.5-μg Pam_3CSK_4 by i.d. injection or MN application in the ear pinna. This location drains to cervical LNs, which were collected on days 7, 14, or 21 postprime for specified studies. Blood was collected every 2 wk (retro-orbital or submandibular, 100 μL) in serum separator tubes (BD Corporation). Sera was stored at −20 °C until analysis.

MD39 Trimer Visualization in Skin and LNs. MD39 was labeled with NHS-functionalized AlexaFluor 647 per manufacturer's protocol (Life Technologies). Mice were immunized as described above. On days 7, 10, or 14 post prime, a set of mice was killed, and skin was collected for imaging. To another group, on days 6 or 13 postprime, 6 μg of anti-CD21/CD35 BV421 antibody (clone 8C12, BD Biosciences) was injected i.v. to label FDCs in situ (40). Mice were killed 24 h later, and cervical LNs were harvested. The LNs and skin were fixed (4% paraformaldehyde, 48 h) and processed by 3DISCO-tissue clearing method (41) to visualize trimer and FDCs by confocal imaging (Olympus Fluoview FV1200, 4× objective). Z-stack images (15 μm/slice, 15–20 slices covering the entire LN) were analyzed by Fiji image analysis software. Briefly, the region of interest (ROI) based on CD35 staining was applied to a trimer-AF647 channel per slice. Raw integrated density (IntDen) of AF647 within this ROI was added together slice by slice through the entire LN to provide a fraction of trimer signal colocalizing with CD35. The total trimer signal was calculated by drawing the outer boundary of the LN and

quantifying raw IntDen of AF647. The sums of intensity projections of the entire z stack were prepared to show MD39 trimer distribution along with FDC clusters in LNs or to visualize MD39 in the skin.

ELISA. Maxisorp 96-well plates (Nunc) were coated with rabbit anti-6xHis tag antibody (Genscript, A00174) or anti-STII (Novus Biologicals, NBP2-41073) at 2 μg/mL in PBS for 4 h at 25 °C and blocked with PBS containing 5% nonfat milk, 10% goat serum, 1% BSA, 1% FBS, and 0.2% Tween 20 or with 1% BSA, respectively, overnight at 4 °C. Plates were coated with MD39-6x His or MD39-STII, respectively, in blocking buffer for 2 h at 25 °C. Serially diluted serum samples were added to plates for 2 h at 25 °C followed by the addition of goat–anti-mouse affinity purified IgG (H+L)-HRP (1:5,000, BioRad,170-6516) for 1 h at 25 °C. Plates were developed with 3, 3′, 5, 5′-tetramethylbenzidine (1-Step Ultra TMB-ELISA substrate solution, ThermoFisher, 34028). The reaction was stopped with 2N sulfuric acid (VWR Analytical). Absorbances were read at 450 and 520 nm (Tecan M1000). Analysis included background subtraction of absorbance at 520 nm from the reading at 450 nm and defining titers as inverse serum dilution where absorbances fell below 0.3.

Flow Cytometry. Cervical LNs were harvested, and single cell suspensions were obtained by treatment with RPMI containing collagenase/dispase (0.8 mg/mL, Sigma-Aldrich) and DNase I (0.1 mg/mL, Sigma-Aldrich) followed by passage through a 70-μm filter (BD Biosciences). Cells were labeled with Live/Dead Aqua (Life Technologies), treated with anti-CD16/21 (Biolegend), and followed by staining with antibodies as in *SI Appendix*, Table S1. For Tfh staining, 2.5×10^5 cells were cultured for 18 h with a peptide pool (15mers overlapping by 11 amino acids) covering the MD39 sequence (5 μg/mL) followed by staining as in *SI Appendix*, Table S1b. Samples were run on a BD Fortessa and analyzed using FlowJo version 10.2.

ELISPOT. BM cells were harvested at 2-mo postboost. Mouse IgG single-color ELISPOT plates (Immunospot) were coated with either total murine Ig capture antibody per manufacturer's instructions or MD39 (5 μg/mL) overnight at 4 °C. BM cells (0.5×10^6) were added to plates in triplicate and cultured for 5 h at 37 °C to determine the total number of ASCs or MD39-specific ASCs, respectively. To determine memory B cell frequency, BM cells (0.5×10^6) were cultured in U-bottom plates with a polyclonal B cell activator (B-poly-S, a mixture of resiquimod and mouse IL2, Immunospot) for 3 d at 37 °C in triplicate and added to plates coated as above. Plates were developed per manufacturer's instructions and spots quantified using an ImmunoSpot S6 Micro Core Analyzer.

Statistical Analysis. All data are plotted as mean ± SEM. All statistical analysis was performed using GraphPad Prism 7.0a. Multivariate comparisons were made by 1-way ANOVA with the appropriate posttest as indicated in the captions with $P < 0.05$ considered significant.

ACKNOWLEDGMENTS. We thank the Koch Institute Swanson Biotechnology Center for Flow Cytometry, Microscopy, and Animal Imaging & Preclinical Testing Core Facilities for technical support. We thank Sudha Kumari and Talar Tokatlian for technical expertise and advice. This work was supported, in part, by the National Institute of Allergy and Infectious Diseases of the NIH under Awards UM1AI100663 and AI104715, Koch Institute Support Grant P30-CA14051 from the National Cancer Institute, International AIDS Vaccine Initiative, and the Ragon Institute of Massachusetts General Hospital, MIT, and Harvard and, in part, by Vaxess Technologies, Inc. The content is solely the responsibility of the authors and does not necessarily represent the official views of the NIH. D.J.I. is an investigator of the Howard Hughes Medical Institute.

1. B. F. Haynes, D. R. Burton, Developing an HIV vaccine. *Science* **355**, 1129–1130 (2017).
2. N. A. Doria-Rose *et al.*; NISC Comparative Sequencing Program, Developmental pathway for potent V1V2-directed HIV-neutralizing antibodies. *Nature* **509**, 55–62 (2014).
3. D. Sok *et al.*, Recombinant HIV envelope trimer selects for quaternary-dependent antibodies targeting the trimer apex. *Proc. Natl. Acad. Sci. U.S.A.* **111**, 17624–17629 (2014).
4. L. M. Walker *et al.*; Protocol G Principal Investigators, Broad neutralization coverage of HIV by multiple highly potent antibodies. *Nature* **477**, 466–470 (2011).
5. J. K. Hu *et al.*, Murine antibody responses to cleaved soluble HIV-1 envelope trimers are highly restricted in specificity. *J. Virol.* **89**, 10383–10398 (2015).
6. H. H. Tam *et al.*, Sustained antigen availability during germinal center initiation enhances antibody responses to vaccination. *Proc. Natl. Acad. Sci. U.S.A.* **113**, E6639–E6648 (2016).
7. P. Schipper *et al.*, Repeated fractional intradermal dosing of an inactivated polio vaccine by a single hollow microneedle leads to superior immune responses. *J. Control. Release* **242**, 141–147 (2016).
8. M. Pauthner *et al.*, Elicitation of robust tier 2 neutralizing antibody responses in nonhuman primates by HIV envelope trimer immunization using optimized approaches. *Immunity* **46**, 1073–1088.e6 (2017).
9. J. Arya *et al.*, Tolerability, usability and acceptability of dissolving microneedle patch administration in human subjects. *Biomaterials* **128**, 1–7 (2017).
10. G. J. P. Fernando *et al.*, Safety, tolerability, acceptability and immunogenicity of an influenza vaccine delivered to human skin by a novel high-density microprojection array patch (Nanopatch™). *Vaccine* **36**, 3779–3788 (2018).
11. N. G. Rouphael *et al.*; TIV-MNP 2015 Study Group, The safety, immunogenicity, and acceptability of inactivated influenza vaccine delivered by microneedle patch (TIV-MNP 2015): A randomised, partly blinded, placebo-controlled, phase 1 trial. *Lancet* **390**, 649–658 (2017).
12. P. C. DeMuth, Y. Min, D. J. Irvine, P. T. Hammond, Implantable silk composite microneedles for programmable vaccine release kinetics and enhanced immunogenicity in transcutaneous immunization. *Adv. Healthc. Mater.* **3**, 47–58 (2014).
13. X. Hu *et al.*, Regulation of silk material structure by temperature-controlled water vapor annealing. *Biomacromolecules* **12**, 1686–1696 (2011).
14. T. Yucel, M. L. Lovett, D. L. Kaplan, Silk-based biomaterials for sustained drug delivery. *J. Control. Release* **190**, 381–397 (2014).
15. R. W. Sanders *et al.*, A next-generation cleaved, soluble HIV-1 Env trimer, BG505 SOSIP.664 gp140, expresses multiple epitopes for broadly neutralizing but not non-neutralizing antibodies. *PLoS Pathog.* **9**, e1003618 (2013).
16. R. W. Sanders *et al.*, HIV-1 VACCINES. HIV-1 neutralizing antibodies induced by native-like envelope trimers. *Science* **349**, aac4223 (2015).
17. M. C. Lebre *et al.*, Human keratinocytes express functional Toll-like receptor 3, 4, 5, and 9. *J. Invest. Dermatol.* **127**, 331–341 (2007).
18. K. Matthews, N. P. Chung, P. J. Klasse, J. P. Moore, R. W. Sanders, Potent induction of antibody-secreting B cells by human dermal-derived CD14+ dendritic cells triggered by dual TLR ligation. *J. Immunol.* **189**, 5729–5744 (2012).
19. D. J. Hines, D. L. Kaplan, Mechanisms of controlled release from silk fibroin films. *Biomacromolecules* **12**, 804–812 (2011).
20. B. D. Lawrence *et al.*, Effect of hydration on silk film material properties. *Macromol. Biosci.* **10**, 393–403 (2010).
21. Q. Lu *et al.*, Water-insoluble silk films with silk I structure. *Acta Biomater.* **6**, 1380–1387 (2010).
22. S. Lau, J. Fei, H. Liu, W. Chen, R. Liu, Multilayered pyramidal dissolving microneedle patches with flexible pedestals for improving effective drug delivery. *J. Control. Release* **265**, 113–119 (2017).
23. A. B. Li, J. A. Kluge, N. A. Guziewicz, F. G. Omenetto, D. L. Kaplan, Silk-based stabilization of biomacromolecules. *J. Control. Release* **219**, 416–430 (2015).
24. D. W. Kulp *et al.*, Structure-based design of native-like HIV-1 envelope trimers to silence non-neutralizing epitopes and eliminate CD4 binding. *Nat. Commun.* **8**, 1655 (2017).
25. C. Havenar-Daughton *et al.*, Cytokine-independent detection of antigen-specific germinal center T follicular helper cells in immunized nonhuman primates using a live cell activation-induced marker technique. *J. Immunol.* **197**, 994–1002 (2016).
26. L. J. Berry *et al.*, Transcutaneous immunization with combined cholera toxin and CpG adjuvant protects against Chlamydia muridarum genital tract infection. *Infect. Immun.* **72**, 1019–1028 (2004).
27. C. M. Gockel, S. Bao, K. W. Beagley, Transcutaneous immunization induces mucosal and systemic immunity: A potent method for targeting immunity to the female reproductive tract. *Mol. Immunol.* **37**, 537–544 (2000).
28. M. G. Pauthner *et al.*, Vaccine-induced protection from homologous tier 2 SHIV challenge in nonhuman primates depends on serum-neutralizing antibody titers. *Immunity* **50**, 241–252 (2019).
29. B. F. Haynes, J. R. Mascola, The quest for an antibody-based HIV vaccine. *Immunol. Rev.* **275**, 5–10 (2017).
30. N. Kasoju, U. Bora, Silk fibroin in tissue engineering. *Adv. Healthc. Mater.* **1**, 393–412 (2012).
31. E. Wenk, H. P. Merkle, L. Meinel, Silk fibroin as a vehicle for drug delivery applications. *J. Control. Release* **150**, 128–141 (2011).
32. E. M. Pritchard, D. L. Kaplan, Silk fibroin biomaterials for controlled release drug delivery. *Expert Opin. Drug Deliv.* **8**, 797–811 (2011).
33. L. Uebersax *et al.*, Silk fibroin matrices for the controlled release of nerve growth factor (NGF). *Biomaterials* **28**, 4449–4460 (2007).
34. A. R. Reeves, K. L. Spiller, D. O. Freytes, G. Vunjak-Novakovic, D. L. Kaplan, Controlled release of cytokines using silk-biomaterials for macrophage polarization. *Biomaterials* **73**, 272–283 (2015).
35. N. Guziewicz, A. Best, B. Perez-Ramirez, D. L. Kaplan, Lyophilized silk fibroin hydrogels for the sustained local delivery of therapeutic monoclonal antibodies. *Biomaterials* **32**, 2642–2650 (2011).
36. X. Wang *et al.*, Silk microspheres for encapsulation and controlled release. *J. Control. Release* **117**, 360–370 (2007).
37. Q. Lu *et al.*, Stabilization and release of enzymes from silk films. *Macromol. Biosci.* **10**, 359–368 (2010).
38. M. R. Prausnitz, Engineering microneedle patches for vaccination and drug delivery to skin. *Annu. Rev. Chem. Biomol. Eng.* **8**, 177–200 (2017).
39. D. N. Rockwood *et al.*, Materials fabrication from Bombyx mori silk fibroin. *Nat. Protoc.* **6**, 1612–1631 (2011).
40. D. Suan *et al.*, T follicular helper cells have distinct modes of migration and molecular signatures in naive and memory immune responses. *Immunity* **42**, 704–718 (2015).
41. A. Ertürk *et al.*, Three-dimensional imaging of solvent-cleared organs using 3DISCO. *Nat. Protoc.* **7**, 1983–1995 (2012).

SI Appendix

Enhancing humoral immunity via sustained-release implantable microneedle patch vaccination

Authors

Archana V. Boopathy[a], Anasuya Mandal[a,b], Daniel W. Kulp[c,d,e], Sergey Menis[c,e,f], Nitasha R. Bennett[a], Hannah C. Watkins[a], Wade Wang[a,b,g], Jacob T. Martin[a], Nikki T. Thai[a], Yanpu He[a,b], William R. Schief[c,e,f,h], Paula T. Hammond[a,b,1], and Darrell J. Irvine[a,c,g,h,I,j,k,1]

Affiliations

[a]Koch Institute for Integrative Cancer Research, Massachusetts Institute of Technology, Cambridge, MA, 02139;
[b]Department of Chemical Engineering, Massachusetts Institute of Technology, Cambridge, MA, 02139;
[c]Center for HIV/AIDS Vaccine Immunology and Immunogen Discovery, The Scripps Research Institute, La Jolla, CA, 92037;
[d]Vaccine and Immunotherapy Center, The Wistar Institute, Philadelphia, PA,;
[e]International AIDS Vaccine Initiative Neutralizing Antibody Center, The Scripps Research Institute, La Jolla, CA, 92037;
[f]Department of Immunology and Microbial Science, The Scripps Research Institute, La Jolla, CA, 92037;
[g]Institute for Soldier Nanotechnologies, Massachusetts Institute of Technology, Cambridge, MA, 02139;
[h]Ragon Institute of Massachusetts General Hospital, Massachusetts Institute of Technology and Harvard, Cambridge, MA, 02139;
[i]Department of Biological Engineering, Massachusetts Institute of Technology, Cambridge, MA, 02139;
[j]Department of Material Science and Engineering, Massachusetts Institute of Technology, Cambridge, MA, 02139;
[k]Howard Hughes Medical Institute, Chevy Chase, MD, 20815
[1] Corresponding author

SI Appendix Methods:

GPC analysis of silk fibroin. Aqueous Gel Permeation Chromatography (GPC) analysis of silk stock material was performed with a silk concentration of 1-5 mg/mL in 100 mM sodium nitrate, 10 mM phosphate buffer with 20% v/v methanol at 35°C pH 7.4 on a Viscotek GPCmax VE-2001 system equipped with a PL aquagel-OH column and VE-3580 RI detector calibrated with monodisperse poly(ethylene oxide) standards.

ATR-FTIR. Silk films (500 µl of 0.5 wt%) were cast on polypropylene surface and dried for 8h at 25°C. The films were then placed inside a dessicator containing 100ml of methanol in a beaker (Sigma-Aldrich). The dessicator was set under vacuum for 24 h at 25°C for methanol vapor annealing of silk films. FT-IR was performed on untreated and annealed silk films using a Thermo Nicolet Nexus 870 equipped with a KBr beamsplitter, liquid nitrogen cooled MCT-A detector, and DuraSamplIR II ATR accessory (SENSIR). Each sample was recorded for 128 scans and baseline set against a blank recording.

FPLC analysis of trimers released from silk MN. Trimers were taken either from stocks and diluted to 50 µg/mL in PBS (5 µg in 100 µL) or after reconstitution with 100 µL PBS from MN which had been loaded with 5 µg trimer (either SOSIP or MD39). The samples were run on a prepacked Superdex 200 Increase 10/300 GL size-exclusion column on an ÄKTA Pure 25M FPLC system at a flow rate of 1 mL/min in PBS. The UV absorbance was monitored at 220 nm and exported for replotting using GraphPad Prism 7.

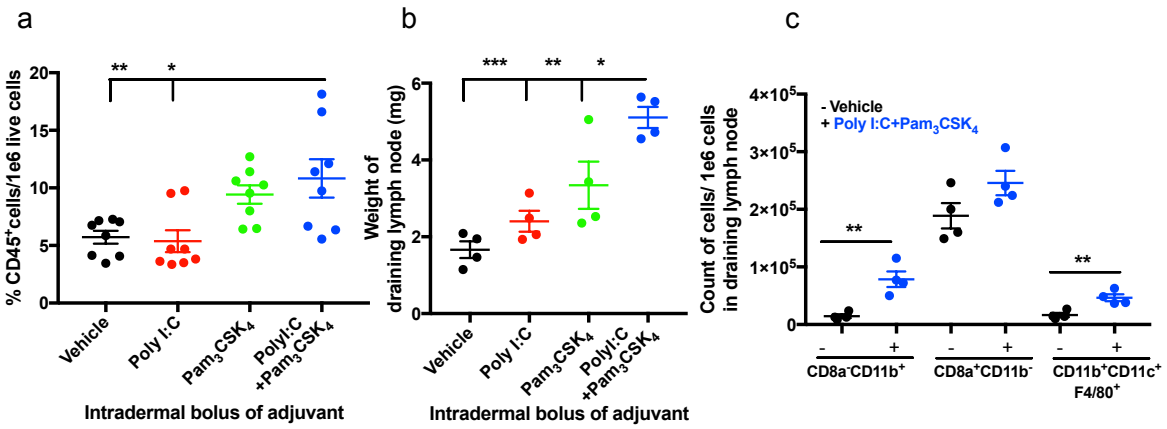

SI Appendix Figure S1. Combination of adjuvants Poly I:C (HMW) and Pam_3CSK_4 recruits more immune cells to the skin and draining lymph node compared to each individual adjuvant. Mice were immunized by intradermal injection of poly I:C, pam_3CSK_4 or a combination of both adjuvants. At 48h post injection, (a) CD45+ cells in the ear skin (b) masses of the draining lymph nodes and (c), quantification of antigen presenting cell subsets in the draining LN. *n*=8/group in a and *n*=4/group in b and c. * p<0.05, ** p<0.01, *** p<0.001. One-way ANOVA in a and b and Student's t-test in c

a

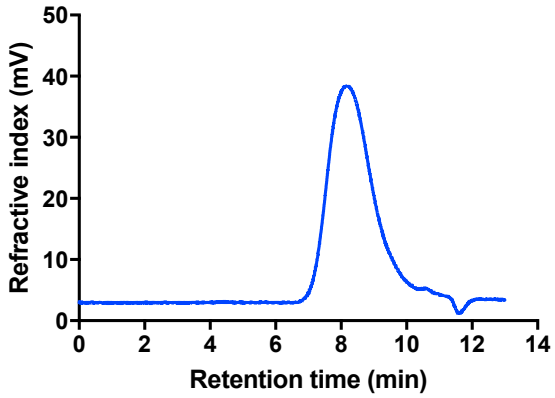

	Mn	Mw	Dispersity (Mw/Mn)
Silk fibroin solution	7810	22680	2.904

b

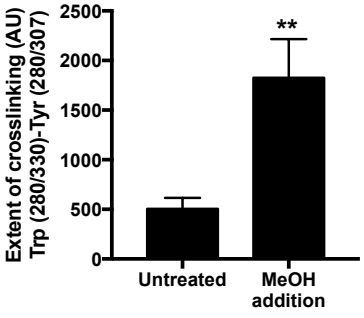

c

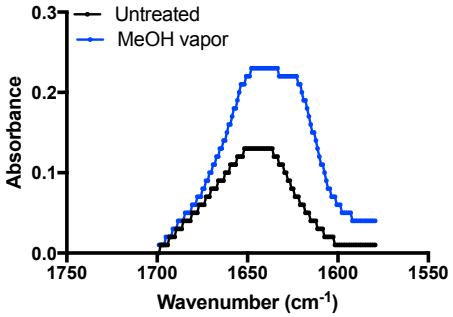

d

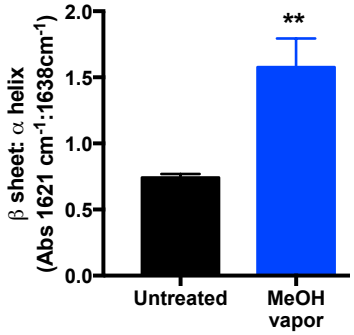

SI Appendix Figure S2. Characterization of silk fibroin. (a) Representative GPC trace of silk fibroin solution boiled for 40 minutes used in microneedles. Table below indicates the molecular weights (in Da) relative to PEG standard. (b) Quantification of silk crosslinking based on beta sheet-dependent fluorescence. (c) Representative FTIR spectra of silk films after MeOH vapor annealing for 24h and (d) quantification of beta-sheet formation. n=2 in a, n=5/group in b, n=4/group in c and d. Student's t-test in b and d. ** $p<0.01$.

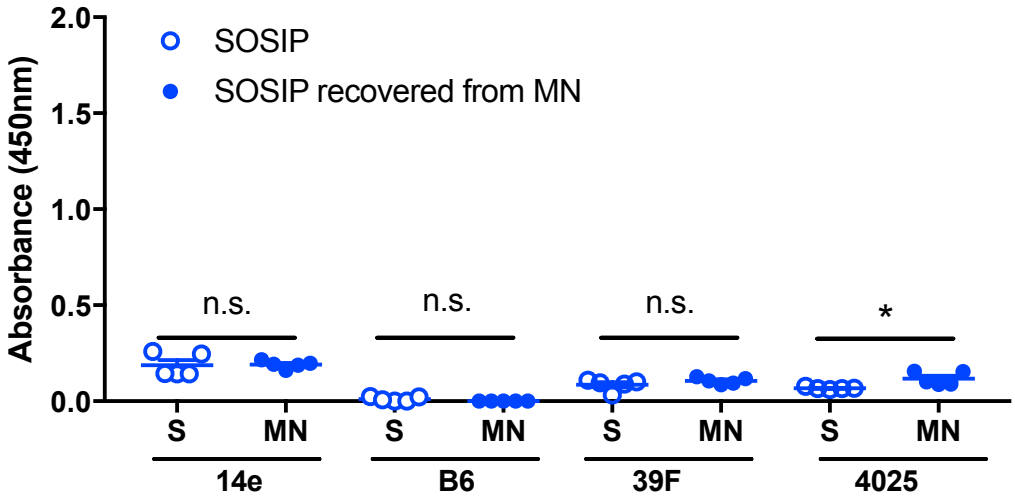

SI Appendix Figure S3. Antigenicity profile of SOSIP. Binding to non-BNabs 14e, B6, 39F are similar between SOSIP recovered from MN (blue circle) and soluble SOSIP (blue open circle) with a small increase in binding to 4025. N=5/group, mean±SEM, n.s. not significant, * $p<0.05$, Student's t-test.

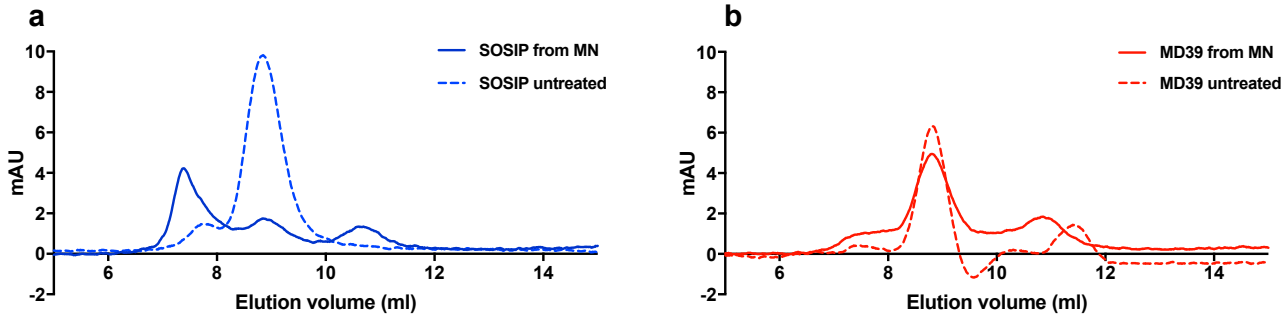

SI Appendix Figure S4: FPLC analysis of trimer released from MNs. Fresh untreated trimers (either SOSIP – panel a or MD39 – panel b) or trimers recovered from MN patches prepared as in Fig. 1c were analyzed on a Superdex 200 FPLC column. Shown are representative elution profiles from groups of 3 patches per condition.

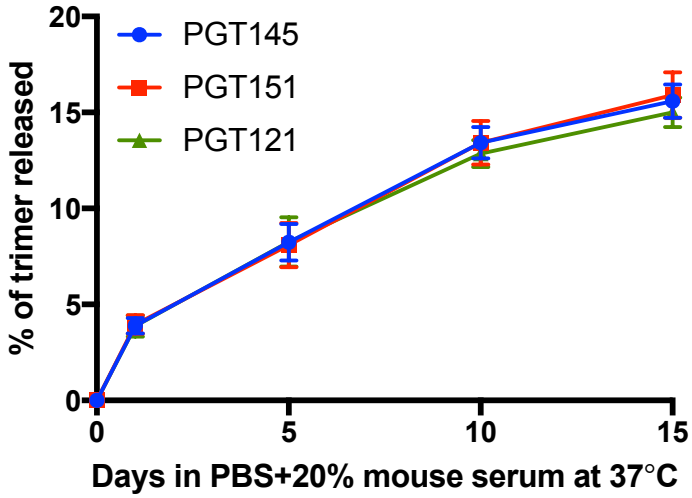

SI Appendix Figure S5. Antigenicity profile of MD39 trimer during sustained release from silk MN patches. Antigenicity profiles of MD39 trimers extracted from as-prepared silk MN were evaluated by capture of recovered trimer on plates followed by ELISA analysis with a panel of bnAbs PGT121, PGT145 or PGT151, normalizing binding to total trimer in MN (*n*=12 patches/group). Shown are mean±SD.

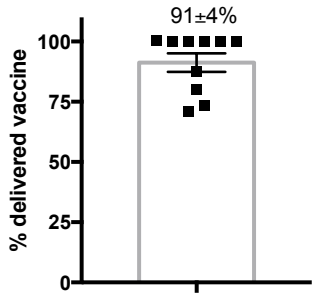

SI Appendix Figure. S6. Measurement of vaccine dose delivered into the skin by MN patches. MNs prepared with Alexa dye-labeled vaccine were imaged by IVIS before and immediately after application to freshly excised mouse skin, and % vaccine delivered was quantified pre and post application. Shown are percentages of total vaccine delivered from replicate MN patches (n=10).

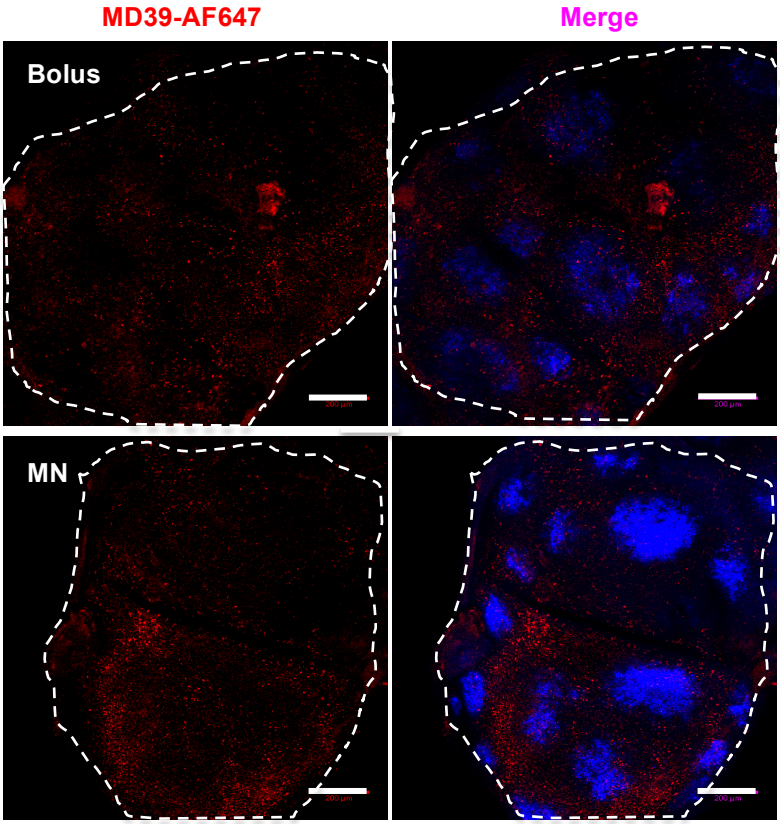

SI Appendix Figure S7. Adjuvant is required for efficient drainage of trimer to lymph node. Mice were immunized with AF647 labeled trimer by bolus injection or MN application. Minimal fluorescent signal associated with trimer (red) was observed in the draining lymph nodes co-stained for CD35, marking FDCs (blue) on day 7 post prime in the absence of adjuvants PolyI:C and pam_3CSK_4. Dotted lines show the outline of the z-projected lymph node imaged by confocal microscopy. n=4/group, Scale bar 200μm.

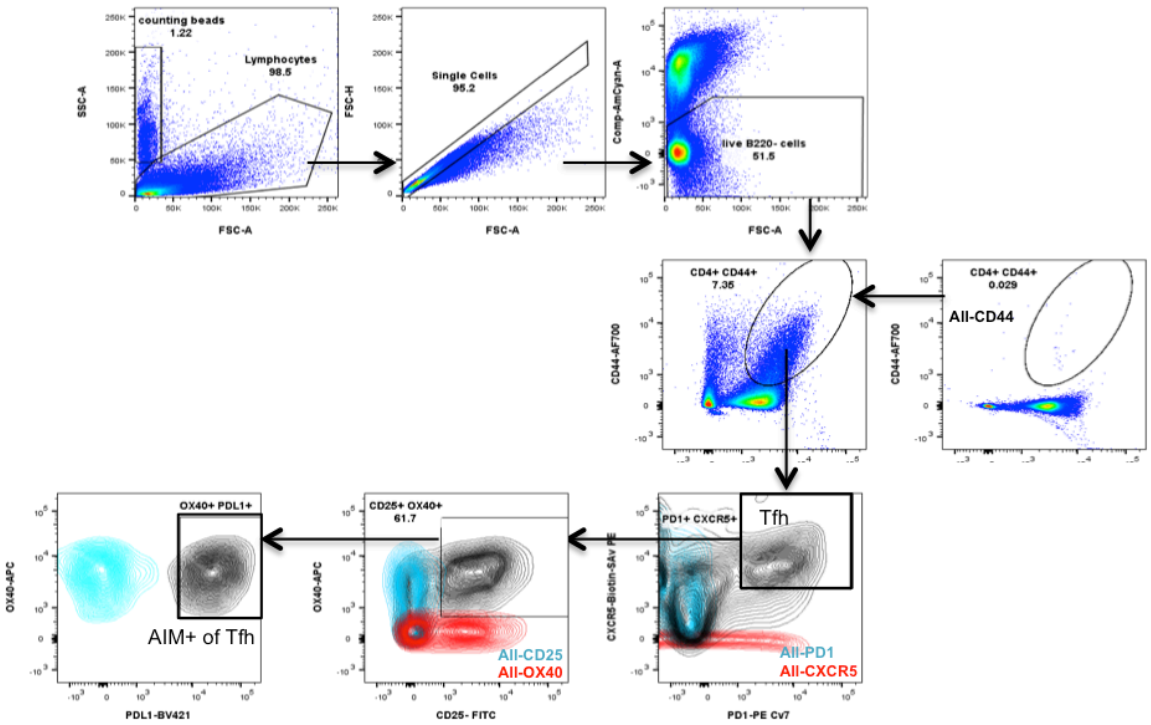

SI Appendix Figure S8. Gating strategy for identification of follicular helper T (Tfh) cells by flow cytometry in the lymph node and activation-induced marker expression. Tfh cells are gated as $B220^{-}CD4^{+}CD44^{+}CXCR5^{+}PD1^{+}$ cells and trimer specific Tfh are a subset of Tfh that are $OX40^{+}CD25^{+}PDL1^{+}$. Fluorescent controls for all fluorophores in the sample except one indicated on the histogram are indicated as All-marker.

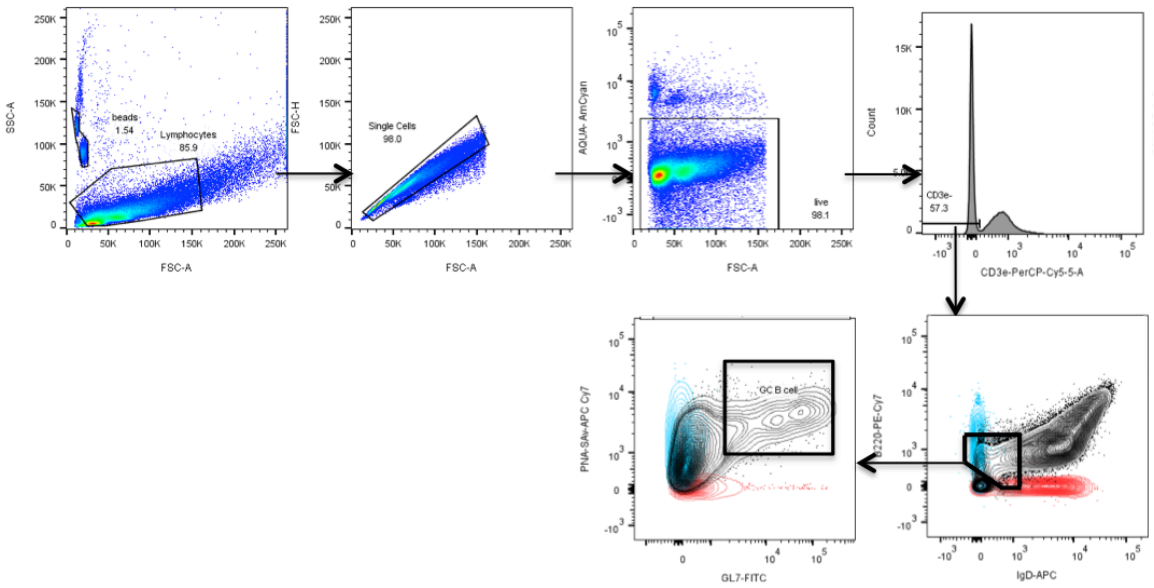

SI Appendix Figure S9. Gating strategy for identification of germinal center (GC) B cells by flow cytometry in the lymph node. GC B cells are gated as $CD3e^{-}B220^{+}IgD^{lo}PNA^{+}GL7^{+}$ cells.

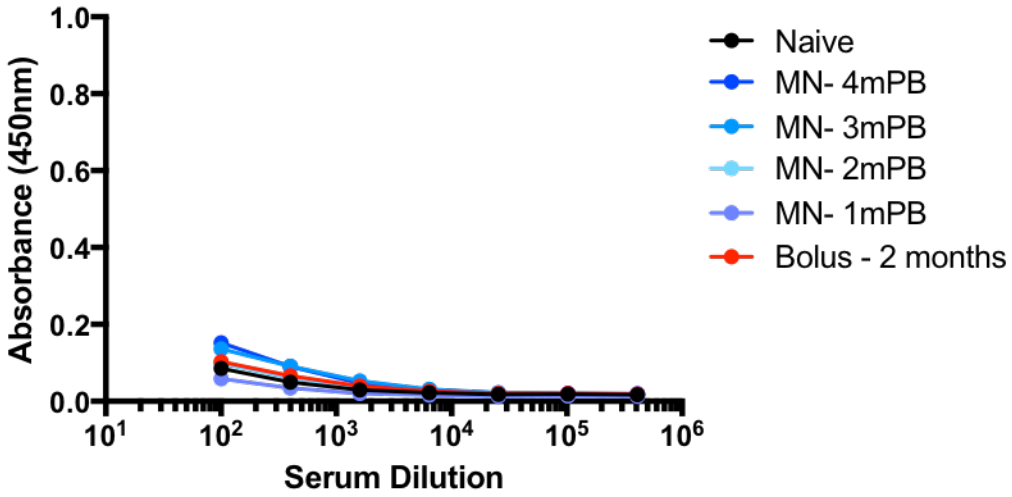

SI Appendix Figure S10. Silk microneedle immunization does not induce silk-specific IgG. Sera of mice immunized by either MN or bolus injections in Figure 4 was analyzed for anti-silk IgG titers. Briefly, ELISA plates were coated with 4µg/ml of silk fibroin in PBS for 2h at RT followed by blocking in PBS+1% BSA for 1h at 37°C. Sera dilutions were added in blocking buffer for 1h at 37°C followed by goat-anti mouse IgG HRP (1:5000, 1h, 37C) and detection using a TMB substrate. Titers following microneedle (MN, in blue) immunization at 1,2,3 and 4 months post boost (mPB) are comparable to mice that were not immunized with silk (bolus, in red) indicating lack of silk-specific IgG induction through microneedle immunization. n=5 animals/group.

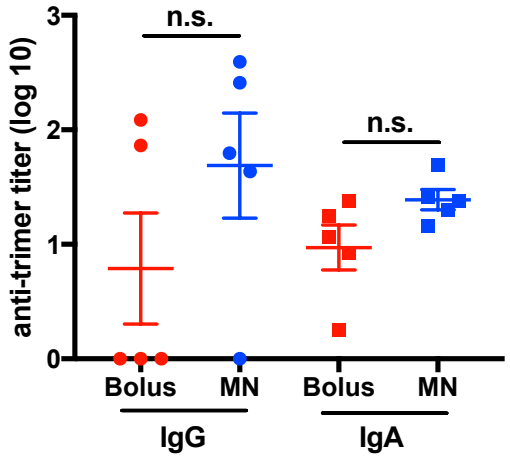

SI Appendix Figure S11. Mucosal anti-trimer IgG and IgA titers at two months post boost in vaginal secretions. n=5/group. n.s. not significant.

SI Appendix Table 1. Antibodies used in flow cytometry experiments are listed below.

Table 1a) GC B cell panel:

Antibody	Flurophore	Dilution	Company	Clone
B220	PECy7	1:200	Biolegend	RA3-6B2
CD3e	PerCPCy5.5	1:100	BDPharmingen	145-2C11
IgD	APC	1:200	eBioscience	11-26c
GL7	FITC	1:100	Biolegend	GL7
PNA	Biotin	1:100	VectorLabs	-
Streptavidin	APCCy7	1:200	BDPharmingen	-

Table 1b) Tfh panel:

Antibody	Flurophore	Dilution	Company	Clone
B220	BV510	1:200	BDHorizon	RA3-6B2
CD44	AF700	1:100	Biolegend	IM7
CD4	PerCPCy5.5	1:100	eBioscience	RM4-5
PD1	PECy7	1:100	eBioscience	J43
Rat anti mouse CXCR5	Pure	1:100	BDPharmingen	2G8
Goat-anti rat	Biotin	1:200	Jackson Immunoresearch	-
Streptavidin	PE		Biorad	-
CD25	FITC	1:100	Biolegend	3C7
OX40	APC	1:100	Biolegend	OX-86
PDL1	BV421	1:100	Biolegend	10F.9G2